Laser-stimulated photodetachment of electrons from the negatively charged dielectric substrates

Y. Ussenov[1,*], M. N. Shneider[2], S. Yatom[1], and Y. Raitses[1]

[1] *Princeton Plasma Physics Laboratory, Princeton University, Princeton, NJ, USA*

[2] *Department of Mechanical and Aerospace Engineering, Princeton University, Princeton, NJ, USA*

**Author for correspondence, e-mail: yussenov@pppl.gov*

Abstract

The photon stimulated emission of bulk electrons has been extensively studied for various types of materials, while photodetachment of surplus surface electrons has not been fully explored. The photodetachment barrier energy is commonly defined by the surface electron affinity of material which is typically less than the work function and more pronounced for non-conducting substrates and in environments with a continuous flux of electrons to the surface, such as in gas discharge plasmas. Herein, it is experimentally shown that the photodetachment yield of surplus electrons created by plasma-induced charging of non-conductive surfaces of dielectric materials depends on the initial surface charge density and do not correlate with the tabulated affinity values of these materials under gas discharge charging conditions. This result obtained using laser stimulated photodetachment for fused silica, boron nitride, and alumina, is critically important for the understanding of charging and discharging dynamics, secondary electron emission, and photo emission effects affecting plasma-wall interactions relevant to surface and capacitively coupled discharges, dusty plasmas, electrostatic probe diagnostics and applications for plasma processing of materials, plasma propulsion and gas breakdown.

The charging and discharging dynamics of non-conductive materials by plasmas is involved in plasma-surface interactions[1] and related interface phenomena[2]. This phenomenon is relevant to widespread applications of various semiconducting and insulating materials as plasma-confined walls[3], substrates for materials processing (e.g., silicon wafers)[4,5,6,7] and electrically insulating holders for diagnostic equipment such as for example, electrostatic probes[8].

Additionally, it plays a crucial role in plasma discharges supported or affected by secondary electron emission (SEE) from dielectric materials such as dielectric barrier[9] discharge (DBD) and capacitively coupled discharges, and plasmas for space applications[10,11] .

The SEE from plasma-facing materials, triggered by ions, electrons[12,13], and photons[14], is key to discharge breakdown, sheath formation[15,16], and ionization balance[17]. While ion- and electron-induced SEE is well-studied[18,19], photon-stimulated electron detachment, especially in dielectrics, is often overlooked. For instance, the energy threshold for electron detachment in dielectrics can impact plasma processes like ion surface recombination and negative ion formation.

The laser-stimulated photodetachment (LSPD) is a technique widely employed for studies of negative ions in plasmas and ion beams[20] and can also be applied for the planar surfaces. In Ref. [21], the photodetachment from the SiO_2 electrode surface of DBD induced a discharge transition from glow to Townsend mode. The threshold binding energy of the surface charge electrons was assumed to be ~ 1.17-2.33 eV, while the electron affinity of the SiO_2 ~ 0.9-1.3 eV. The photodetachment yield was estimated to be ~10^{-8}, but the actual values of yield and cross sections were not determined because of uncertainties in the laser beam shape. In another study, the impact of photodetachment of surplus negative charges from alumina surface by discharge-generated photons predicted to be the trigger for the streamer formation from opposite electrodes of the DBD[22]. The binding energy is assumed to be lower than 3.5 eV, while theoretical estimations[23] and thermal desorption studies from the alumina lead in prediction of the binding energy of electrons as ~1 eV[24,25]. The LSPD was also applied for diagnostics of particle charge[26,27,28]. In Ref.[27], the effect of the thermal emission found to be negligible on the detachment of electrons, however the role of photoemission and photodetachment is not clearly defined as the photon energy was close to the work function of common dielectric materials.

Although the photoemission is a well-studied for various types of materials, the photo detachment has not been deeply investigated. In all relevant previous studies, the clear distinction between photoemission and photodetachment in the visible wavelength range, and their role in SEE from plasma-charged dielectric surfaces was not explored in detail. Photodetachment differs from photoemission in that the emitted electrons come from the surface, where they were previously attached, rather than from the bulk material. While the threshold energy for photoemission is determined by the work function of the material, photodetachment is

governed by the surface's electron affinity. Typically, electron affinity is lower than the work function, suggesting that detachment of electrons from charged surfaces is more intense, even at photon energies below the work function. Commonly accepted hypotheses relying on the assumption of "tabulated" surface electron affinity of clean materials as the threshold value needs to be tested for real dielectric materials widely used in gas discharge plasma applications[29,30].

In this letter, the LSPD of electrons from plasma-charged dielectric substrates such as alumina (Al_2O_3), fused silica (SiO_2), and hexagonal boron nitride (h-BN) has been studied. Laser pulses with photon energies of 2.33 eV and 3.49 eV were applied to minimize bulk electron photoemission. The obtained photodetachment yield and cross sections have been analyzed in relation to the tabulated electron affinities χ of used dielectric samples (Table 1). The detachment of surface surplus electrons, including yield and cross-section, has not been thoroughly studied for planar substrates, even though bulk electron emission has been well explored. While photoemission studies typically use high-energy photons, the effect of low-energy photons on the detachment of less tightly bound surface electrons remains underexplored. Our study aims to quantitatively define the yield and cross-section of surplus surface electron detachment by low-energy photons and correlate these with electron affinities for common dielectric materials relevant to plasma processing. The data on LSPD provides valuable insights for simulating surface charging and discharging dynamics, while the technique itself serves as a promising diagnostic tool for monitoring and managing surface charges. The results also suggest that by carefully adjusting the flux of low-energy laser photons, it is possible to control or even eliminate surface electron charge density with minimal damage to the substrates.

Table 1. Tabulated electron affinities and relative permittivity of studied dielectric materials

Material	Rel. permittivity	Diameter, mm	Thickness, mm	χ, eV
SiO_2	3.8	25.4	1.56	0.9-1.3[30,31]
Al_2O_3	9.5	25.4	1.56	1.9-2.5[30,31]
h-BN	4.0	25.4	1.90	1.14 - 1.34[32]

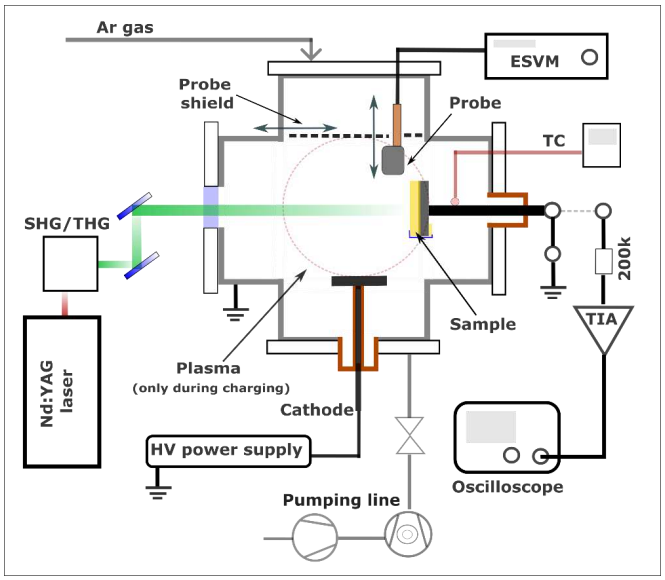

Figure 1. The general scheme of the experimental setup

The experimental setup is shown in Figure 1. The industrial-grade SiO_2 (Momentive Tech., 99.9%), Al_2O_3 (Coors Tek Inc., 99.5%) and h-BN (Momentive Tech., 95%) samples, are fixed on the metallic substrate holder isolated from the chamber walls. The selection of Al_2O_3, SiO_2, and h-BN as test substrates is driven by their common use as insulators in plasma science and technology, microelectronics, aerospace and triboelectric applications, their availability with well-documented properties, and their differing electron affinities, enabling correlation studies with LSPD yield and cross-section. The samples cleaned in acetone, ethyl alcohol and distilled water to remove the surface contaminants. To eliminate the physiosorbed water from the surface, the samples heated up to ~180-200°C under the ~$5x10^{-7}$ Torr pressure for several hours. Preliminary laser beam exposures of samples were conducted at high laser fluences under the vacuum to remove the rest of the impurities from the surface and ensure good reproducibility of measurements.

The dielectric samples charged by DC glow discharge (V_{dis} = -450 V, I_{dis} = 1.5 ± 0.3 mA) in 100 mTorr Argon (99.999%) plasma. The plasma was used only for the initial charging of substrates and was turned off during the surface charge decay and photodetached electron current

measurements. The stainless-steel cathode (D=25.4 mm) of the DC discharge was inserted from the opposite side to the electrostatic voltmeter (ESVM) probe (Trek –347) and fixed at a distance of ~ 30 mm from the sample edge, while the grounded chamber wall served as the anode of the discharge.

For the LSPD, the second (SH) and third (TH) harmonics of the Nd:YAG laser (beam diameter ~ 9 mm, pulse frequency 10 Hz, and a pulse width is ~9 ns) with wavelengths of 532 nm ($h\nu$ = 2.33 eV) and 355 nm ($h\nu$ = 3.49 eV) are exposed perpendicular to the sample surface through a glass viewport. Although the non-contact ESVM probe measurements do not directly depend on the probe-to-surface distance[33], the probe tip is positioned perpendicular to the substrate surface with a 1.0 ± 0.3 mm gap, as recommended by the manufacturer. The center of the probe tip box is aligned with the center of the laser beam spot on the substrate surface. During plasma charging, the ESVM probe head is retracted, and a metallic shield plate is placed between the probe and the discharge region. The photodetached electron current from the samples was measured by the homemade transimpedance amplifier (TIA) for the first five laser pulses at 355 nm laser wavelength. The TIA is connected to the substrate holder via a 200 kΩ resistor and current signals are recorded by an oscilloscope (Siglent - SDS2354, 350 MHz, 2 Gs/s).

Figure 2 shows the surface potential decay for the dielectric samples during the continuous laser exposure with 532 nm and 355 nm wavelength and 0.030 J/cm^2 and 0.019 J/cm^2 beam fluence respectively. After plasma charging the surface potential of all samples was $V_{surf} = -31.0 \pm 4\,V$ (both for the ESVM and TIA current measurements) that is due to charging by plasma electrons. The negative surface potential decay rate with 532 nm laser exposure is fast for the first $\sim 10^3$ of laser shots leading to the reduction (in absolute value) of the surface potential down to $V_{surf} \sim -17.5\,V$ for Al_2O_3 and h-BN and $V_{surf} \sim -28.0\,V$ for SiO_2. Further decay of the surface potential is very slow and after 9.6 x 10^3 pulses it drops no more than $\Delta V_{surf} = 10V$. For the 355 nm laser exposure, the surface potential decay is faster depending on the number of the laser shots, and the discharging time scale in Figure 3 (c) and (d) is an order of magnitude less than that for the 532 nm laser. The first ~200 shots cause the potential drop of about $\Delta V_{surf} = 24V$ for h-BN and Al_2O_3, and $\Delta V_{surf} = 20V$ for SiO_2. The natural surface potential decay measured without laser photodetachment, under the same conditions, shows a reduction in V_{surf} of ~2% for Al_2O_3 and SiO_2, and ~9% for h-BN during the

first 30 minutes, which is negligible compared to the decay induced by LSPD. The corresponding surface electron charge density decay calculated according to the expression $\sigma_e = \Delta V_{surf} \varepsilon \varepsilon_0 / d$, where ε_0 – electric constant, ε –dielectric permittivity and d – thickness of substrate. Note that the charge density for SiO_2 and h-BN shows the similar value $\sigma_e \approx 3.75 \times 10^{12}\ e/m^2 (-0.6 \frac{\mu C}{m^2})$, while for the Al_2O_3 $\sigma_e \approx 1.03 \times 10^{13}\ e/m^2 (-1.65 \frac{\mu C}{m^2})$ which is almost ~3 times higher due to the large dielectric permittivity (Table 1) at the similar thickness and surface area.

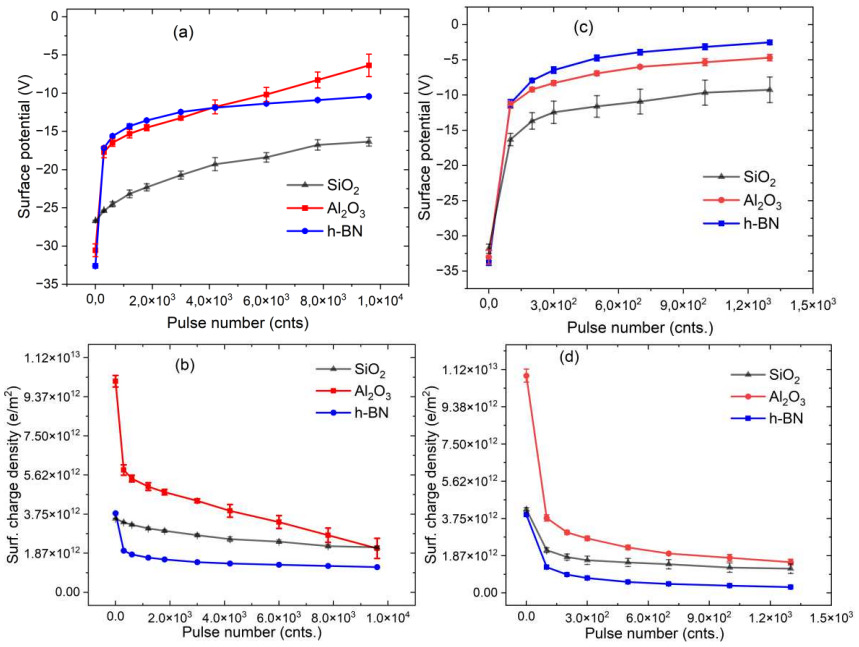

Figure 2. The surface potential and charge density decay for the dielectric samples by LSPD with 532 nm, 0.030 J/cm^2 (a,b) and 355 nm, 0.019 J/cm^2 (c,d) wavelength laser beams.

Figure 2 demonstrates that the LSPD efficiency and the rate of charge decay is not linear depending on laser shots. This behavior indicates that the LSPD yield is not constant and falls after each laser shot. The average yield per pulse is calculated as:

$$\gamma_{pd} = \frac{\sigma_e}{\sigma_{ph}} = \frac{\Delta V_{surf}\, \varepsilon\varepsilon_0\, S_{las}}{d\, e\, dN_{pulse}\, n_{ph.p}}. \quad (1)$$

Here, $\sigma_e = \frac{\Delta Q}{S_s\, e dN_{pulse}} = (\Delta V_{surf}\, \varepsilon\varepsilon_0)/(d\, e\, dN_{pulse})$ is the surface charge density of detached electrons, where $\Delta Q = C\Delta V_{surf}$ is the amount of detached charge at certain number of laser shots, $C = \varepsilon\varepsilon_0 S_s/d$ is the substrate capacitance, S_s is the substrate surface area, e is the elementary charge, dN_{pulse} is the number of laser shots between two subsequent measurements as there is no any replenishment of the surface with electrons from the plasma, $\sigma_{ph} = n_{ph.p}/S_{las}$ is the surface density of incident photons, $n_{ph.p}$ is the number of photons per pulse and S_{las} is the laser beam cross section area.

Examples of the average LSPD yield for different substrate materials and laser photon energy listed in Table 2. The highest photodetachment yield shows the Al_2O_3, then h-BN, and LSPD yield for SiO_2 shows minimum value.

Table 2. The average LSPD yield of samples at different laser photon energy.

Material	355 nm (3.49 eV)	532 nm (2.33 eV)
Al_2O_3	2.06±0.67 x 10^{-10}	1.75±0.35 x 10^{-11}
h-BN	7.46±2.46 x 10^{-11}	7.36±1.47 x 10^{-12}
SiO_2	5.83±1.92 x 10^{-11}	7.27±1.45 x 10^{-13}

The LSPD yields from ESVM measurements were validated by detecting photodetachment-induced electron currents using TIA for 355 nm laser shots. Figure 3(a) shows the initial photodetachment current for different samples. TIA measurements for the first five pulses (figure S1 in Supplementary material) reveal a reduction in detached electrons with subsequent shots, confirming the ESVM results. Figure 3(b) shows normalized photodetachment currents with a consistent decay time of ~5 μs across all samples, indicating that the decay time is determined by the vacuum chamber's capacitance, which is the same for all the case. The detachment yield is defined as:

$$\gamma_{pd} = \frac{n_{ph.det.}}{n_{ph.p}}, \quad (2)$$

where $n_{ph.det.}$ -number of detached electrons in elementary charge units and calculated by $n_{ph.det.} = \int_{t_0}^{t_1} I(t)dt\,/e$, where $I(t)$ -measured photodetachment current, t_0 = 0 μs to t_1 = 15 μs.

Table 3 shows a comparison of the results for the first pulse for all three dielectric samples. The results from both measurements are in reasonable agreement within the experimental error and demonstrate that the Al_2O_3 has the highest LSPD yield and SiO_2 showed the lowest value.

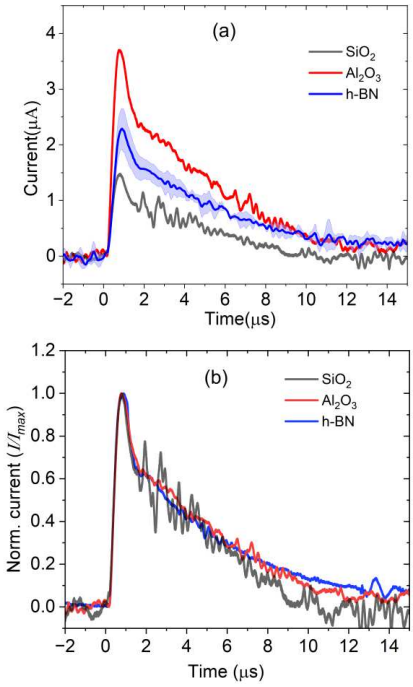

Figure 3. The photodetached electron current measured with TIA after first laser (355 nm) shot (a) and normalized values (b) for different samples. The standard deviation is ±15% and based on the peak value for the h-BN obtained by three measurements.

Table 3. The comparison of LSPD yield for single pulse obtained by ESVM and TIA measurements

Sample	ESVM	TIA
Al_2O_3	4.89±0.83 x 10^{-9}	3.57 ±1.24 x 10^{-9}
h-BN	1.98±0.33 x 10^{-9}	2.81±0.98 x 10^{-9}
SiO_2	4.51±0.9 x 10^{-10}	1.185±0.41 x 10^{-10}

Assuming no recharging of the surface by electrons during and after the surface exposure to the LSPD, the surface charge decay rate from the LSPD can be defined as[34]:

$$\frac{dN_e(t)}{dt} = -\Gamma_{ph}\,\sigma_{pd} N_e(t) \tag{3}$$

$$N_e(t) = N_e(0)\exp\left(\frac{-t}{\tau_{opt}}\right) + N_{e.sat} \tag{4}$$

where N_e – surface density of electrons on the dielectric substrate, $N_{e.sat}$ – density of electrons after saturation of decay, Γ_{ph} -photon flux per unit area, σ_{pd} – photodetachment cross section for given laser photon energy. Then, the photodetachment decay of surface surplus electrons follow the exponential function with time constant defined by the cross section σ_{pd} and photon flux Γ_{ph}:

$$\tau_{opt} = \frac{1}{\sigma_{pd}\Gamma_{ph}} \tag{5}$$

The values of τ_{opt} can be obtained from the fitting results, photon flux obtained for assuming the ~9 ns of laser pulse width, and with assumption that the charge lost between laser pulses is negligible. Fitting the surface charge decay curves shows that a double exponential model better represents the data, suggesting two possible underlying photodetachment mechanisms. Figure 4 presents the double exponential fit, with cross sections σ_{pd1} and σ_{pd2} in Table 4. For comparison, single exponential fit results are in Figure S2 and Table S1 of the Supplementary Material. The first decay cross section σ_{pd1} is attributed to the photodetachment from the materials surface. Indeed, the σ_{pd1} in the range of ~ 10^{-24} m^2 and 10^{-22} m^2 for the 532 nm ($h\nu$ =2.33 eV) and 355 nm ($h\nu$ = 3.49 eV) lasers respectively, and they correlate with the γ_{pd} showing the largest value for Al_2O_3 and h-BN, and the lowest value for the SiO_2. The second decay cross sections σ_{pd2} about an order of magnitude lower than σ_{pd1}, and no correlation is

observed among the type of materials and photon energies. Simple estimates (details in Supplementary Material) show that the laser pulse raises the surface temperature by no more than ΔT_{max}~250K, suggesting thermal effects are unlikely to cause electron detachment at larger accumulated pulse numbers. We speculate that the second fit parameter in the charge decay curves relates to the detachment of electrons from surface-bound negative ions, like OH^-, rather than from the material itself. Further investigation of this mechanisms would require advanced surface characterization under UHV conditions, which is beyond this study's scope. Double exponential natural charge decay after dielectric barrier discharge was previously seen in BSO crystals[35], and attributed to photoconductivity and surrounding gas conditions. However, this doesn't apply here, as our materials are non-photoconductive, and the environment is a low-pressure vacuum with Argon.

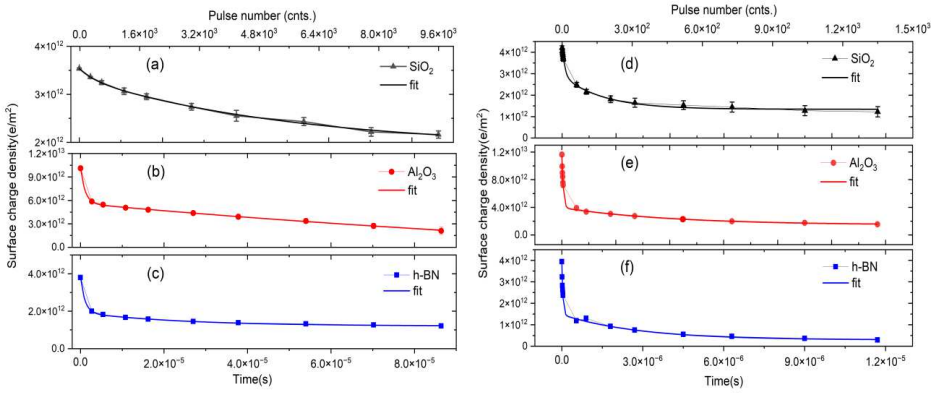

Figure 4. Fitting examples of LSPD induced electronic surface charge decay curves for different dielectric samples for 532 nm (a,b,c) and 355 nm (d,e,f) laser beams.

Table 4. The average LSPD cross-section σ_{pd1} and σ_{pd2} for different samples.

Material	355 nm (3.49 eV), m^2		532 nm (2.33 eV), m^2	
	σ_{pd1}	σ_{pd2}	σ_{pd1}	σ_{pd2}
SiO_2	2.45±0.31 x 10^{-22}	1.61±0.24 x 10^{-23}	2.98±0.93 x 10^{-24}	2.15±0.42 x 10^{-25}
Al_2O_3	4.78±0.28 x 10^{-22}	5.90±0.88 x 10^{-24}	9.87±0.92 x 10^{-24}	5.84±2.46 x 10^{-26}

h-BN	6.04±0.775 x 10^{-22}	8.57±2.51 x 10^{-24}	1.03±0.13 x 10^{-23}	4.44±0.47 x 10^{-25}

The LSPD from different samples shows that the photodetachment yield depends both on the material itself and on the initial (or remaining) surface charge density for the same type of material. Highest yields and cross sections show the Al_2O_3 and h-BN, while the lowest for SiO_2, which is not in correlation with tabulated χ (Table 1).

To explain the nonlinear reduction in surface charge decay rate and γ_{pd} during LSPD, assume a uniform charge distribution. Given that the surface atom density on the crystal plane is ~10^{18} m^{-2} and the incident photon density per laser pulse is ~ 2 - 5 x 10^{16} photons/m^2, the surplus electron density responsible for charging (~4.0 x 10^{12} e/m^2 for SiO_2 and h-BN, and ~10^{13} e/m^2 for Al_2O_3) is much lower than the bulk electrons and incident photons. Surface potential decay measurements (Figure 2) reveal that the number of detached electrons decreases with each laser shot, showing a high decay rate initially, followed by an exponential drop. Analysis of the LSPD-induced current (detected by TIA) at 3.49 eV photon energy supports this. Initially, the high surface electron density leads to more detachment, but as shots continue, the density decreases, reducing detachment probability and lowering γ_{pd}. Thus, photodetachment yield depends on the initial surface electron charge density at a fixed photon count. A similar nonlinear reduction in surface charge decay rate is observed for the discharging of dielectric surfaces through natural charge decay[36] as well as through photon-excited[37] or thermally stimulated decay [38] processes.

One would expect γ_{pd} to follow the trend of lower electron affinity χ leading to a higher yield at a given laser fluence and photon energy, based on the tabulated χ values. The lack of correlation between χ and γ_{pd} may be due to several factors. Firstly, the χ is a surface property that varies greatly due to factors like surface defects, impurities, and exposure to ambient conditions, plasma, or cleaning. Therefore, the effective χ can differ significantly for the same material based on its physicochemical properties, surface treatment, and preparation methods[39,40,41]. Secondly, assuming χ as the binding energy for electron photodetachment overlooks electronic charge traps on the solid surface. These traps, caused by surface defects, dangling bonds, and adatoms, are energy states within the forbidden gap below the conduction band minimum[42]. Finally, the highest γ_{pd} for Al_2O_3 is due to its surface charge density being

about three times larger than that of h-BN and SiO_2, resulting in a higher photodetachment yield at the same incident photon density. Although h-BN and SiO_2 have similar tabulated electron affinities, h-BN shows higher γ_{pd}, likely due to lower χ from surface impurities[43]. In contrast, SiO_2 may have deep charge traps caused by its amorphous nature and high disorder in the surface crystal lattice structure[40,44].

In conclusion, LSPD induced surface charge decay rate from negatively charged dielectric substrates is nonlinear and decreases with subsequent laser shots. This indicates that for the given incident photon flux, the photodetachment yield can be highly affected by the initial (or remaining) density of surface charges. The latter is not true for the simple photoemission process of bulk electrons. The experiments under real gas discharge conditions show that the photodetachment yields and cross sections for Al_2O_3, h-BN, and SiO_2 do not follow the trends of tabulated electron affinity values. LSPD can influence plasma properties by contributing to breakdown, sheath formation, and ionization balance, especially when surface charge density is high due to insulating substrates or high voltage. Adjusting low-energy laser photon flux could control or eliminate surface charges, preventing arcing or damage in plasma processing and space applications. For LSPD diagnostics in dusty plasmas, operating in a fully saturated regime is key to accurately measure particle charge densities, as not all electrons may be removed in a single shot. The obtained photodetachment data can inform modeling and simulations. Future work will focus on the study of LSPD directly in the plasma medium and on the understanding different additional underlaying photodetachment mechanisms, such as laser-stimulated thermal emission, desorption of surface adatoms and detachment from surface negative ions.

Supplementary Material

See the supplementary material for LSPD photodetached current pulses corresponding to different numbers of laser pulses, the results of single exponential decay fitting for LSPD-induced surface charge decay, and estimations of substrate surface heating after a single laser pulse.

Acknowledgements

The authors acknowledge the US Department of Energy (DOE) for support of the work by the contract DE-AC02-09CH11466 and Mr. T. Bennet for providing technical assistance.

Author Declarations

Conflict of Interest

The authors have no conflicts to disclose.

Author Contributions

Y. Ussenov: Data curation (lead); Formal analysis (lead); Investigation (equal); Validation (equal); Writing – original draft (lead); Writing – review & editing (equal). **M. Shneider**: Conceptualization (equal); Investigation (equal); Formal analysis (equal); Writing – review & editing (equal); Supervision (equal). **S. Yatom**: Conceptualization (equal); Investigation (equal); Formal analysis (equal); Writing – review & editing (equal); Supervision (equal). **Y. Raitses**: Conceptualization (equal); Investigation (equal); Formal analysis (equal); Writing – review & editing (equal); Supervision (lead).

Data Availability

The data that support the findings of this study are available from the corresponding author upon reasonable request.

References

[1] F. X. Bronold, K. Rasek, H. Fehske, Electron microphysics at plasma–solid interfaces. *J. Appl. Phys.* **128 (18)** 180908 (2020)

[2] S. M. Rossnagel, J. J. Cuomo and W. D. Westwood, Handbook of Plasma Processing Technology: Fundamentals, Etching, Deposition, and Surface Interactions, Park Ridge: Noyes Publications, (1990)

[3] S. Nemschokmichal, R. Tschiersch, H. Höft, R. Wild, M. Bogaczyk, M. M. Becker, D. Loffhagen, L. Stollenwerk, M. Kettlitz, R. Brandenburg and J. Meichsner, Impact of volume and surface processes on the pre-ionization of dielectric barrier discharges: advanced diagnostics and fluid modeling. *Eur. Phys. J. D***. 72**, 89 (2018)

[4] N. Marchack, L. Buzi, D. B. Farmer, H. Miyazoe, J. M. Papalia, H. Yan, G. Totir, S. U. Engelmann, Plasma processing for advanced microelectronics beyond CMOS. *J. Appl. Phys.* **130 (8)** 080901 (2021)

[5] G. S. Oehrlein and S. Hamaguchi, Foundations of low-temperature plasma enhanced materials synthesis and etching, *Plasma Sources Sci. Technol.* **27** 023001 (2018)

[6] S.-N. Hsiao, M. Sekine, K. Ishikawa, Y. Iijima, Y. Ohya, M. Hori, An approach to reduce surface charging with cryogenic plasma etching using hydrogen-fluoride contained gases, *Appl. Phys. Lett*. **123**, 212106 (2023)

[7] W. Zhu, S. Sridhar, L. Liu, E. Hernandez, V. M. Donnelly, D. J. Economou, Photo-assisted etching of silicon in chlorine- and bromine-containing plasmas, *J. Appl. Phys.* **115**, 203303 (2014)

[8] V. I. Demidov, S. V. Ratynskaia, K. Rypdal, Electric probes for plasmas: The link between theory and instrument, *Rev. Sci. Instrum*. **73**, 3409–3439 (2002)
[9] R. Brandenburg, Dielectric barrier discharges: progress on plasma sources and on the understanding of regimes and single filaments, *Plasma Sources Sci. Technol.* **26** 053001 (2017)
[10] Y. Raitses, A. Smirnov, D. Staack, N. J. Fisch, Measurements of secondary electron emission effects in the Hall thruster discharge, *Phys. Plasmas* **13**, 014502 (2006)
[11] S. T. Lai, Fundamentals of Spacecraft Charging: Spacecraft Interactions with Space Plasmas (Princeton, NJ: Princeton University Press) (2011)
[12] B. Horváth, M. Daksha, I. Korolov, A. Derzsi and J. Schulze, The role of electron induced secondary electron emission from SiO_2 surfaces in capacitively coupled radio frequency plasmas operated at low pressures, *Plasma Sources Sci. Technol.* **26** 124001 (2017)
[13] D.-Q. Wen, J. Krek, J. T. Gudmundsson, E. Kawamura, M. A. Lieberman, P. Zhang, J. P. Verboncoeur, Field reversal in low pressure, unmagnetized radio frequency capacitively coupled argon plasma discharges. *Appl. Phys. Lett.* **123** (26): 264102 (2023)
[14] A. Iqbal, B. Z Bentz, Y. Zhou, K. Youngman and P. Zhang, Pulsed photoemission induced plasma breakdown, *J. Phys. D: Appl. Phys.* **56** 505204 (2023)
[15] M. D. Campanell and M. V. Umansky, Strongly Emitting Surfaces Unable to Float below Plasma Potential, *Phys. Rev. Lett.* **116**, 085003 (2016)
[16] J. P. Sheehan, N. Hershkowitz, I. D. Kaganovich, H. Wang, Y. Raitses, E. V. Barnat, B. R. Weatherford, and D. Sydorenko, Kinetic Theory of Plasma Sheaths Surrounding Electron-Emitting Surfaces, *Phys. Rev. Lett.* **111**, 075002 (2013)
[17] A. V. Phelps and Z Lj Petrovic, Cold-cathode discharges and breakdown in argon: surface and gas phase production of secondary electrons, *Plasma Sources Sci. Technol.* **8** R21 (1999)
[18] A. Ottaviano, S. Banerjee, Y. Raitses; A rapid technique for the determination of secondary electron emission yield from complex surfaces. *J. Appl. Phys.*, **126** (22): 223301 (2019)
[19] A. Dunaevsky, Y. Raitses, N. J. Fisch, Secondary electron emission from dielectric materials of a Hall thruster with segmented electrodes, *Phys. Plasmas* **10**, 2574–2577 (2003)
[20] M. Bacal, Photodetachment diagnostic techniques for measuring negative ion densities and temperatures in plasmas, *Rev. Sci. Instrum.* **71** (11): 3981–4006 (2000)
[21] R. Tschiersch, S. Nemschokmichal and J. Meichsner, Influence of released surface electrons on the pre-ionization of helium barrier discharges: laser photodesorption experiment and 1D fluid simulation, *Plasma Sources Sci. Technol.* **26** 075006 (2017)
[22] O. Guaitella, I. Marinov, A. Rousseau, Role of charge photodesorption in self-synchronized breakdown of surface streamers in air at atmospheric pressure. *Appl. Phys. Lett.* **98** (7): 071502 (2011)
[23] Y.B. Golubovskii, V.A. Maiorov, J. Behnke and J.F. Behnke, Influence of interaction between charged particles and dielectric surface over a homogeneous barrier discharge in nitrogen, *J. Phys. D: Appl. Phys.* **61** 35751(2002)
[24] P. F. Ambrico, M. Ambrico, L. Schiavulli, T. Ligonzo, V. Augelli, Charge trapping induced by plasma in alumina electrode surface investigated by thermoluminescence and optically stimulated luminescence. *Appl. Phys. Lett.*, **94** (5): 051501 (2009)
[25] M. Li, C. Li, H. Zhan, J. Xu, X. Wang, Effect of surface charge trapping on dielectric barrier discharge. *Appl. Phys. Lett.*, **92** (3): 031503 (2008)

[26] E. Stoffels, W. W. Stoffels, G. M. W. Kroesen, F. J. de Hoog, Dust formation and charging in an Ar/SiH_4 radio-frequency discharge, *J. Vac. Sci. Technol. A* **14**, 556–561 (1996)
[27] T. J. A. Staps, T. J. M. A. Donders, B. Platier and J. Beckers, In-situ measurement of dust charge density in nanodusty plasma, *J. Phys. D: Appl. Phys.* **55** 08LT01 (2022)
[28] M. Shneider, Y. Raitses, S. Yatom, Schottky effect on the wavelength threshold for the photo-detachment from charged metallic nanoparticles, *J. Phys. D: Appl. Phys.* **56** (29), 29LT01 (2023); *J. Phys. D: Appl. Phys.* **56** 439501 (2023)
[29] F. X. Bronold and H. Fehske, Absorption of an Electron by a Dielectric Wall, *Phys. Rev. Lett.* **115**, 225001 (2015)
[30] R. L. Heinisch, F. X. Bronold, and H. Fehske, Electron surface layer at the interface of a plasma and a dielectric wall, *Phys. Rev. B* **85**, 075323 (2012)
[31] I. Shlyakhov, J. Chai, M. Yang, S. Wang, V. V. Afanas'ev, M. Houssa, A. Stesmans, Energy band alignment of a monolayer MoS_2 with SiO_2 and Al_2O_3 Insulators from Internal Photoemission, *Phys. Status Solidi A*, **216** 1800616 (2019)
[32] T. Knobloch, Y.Y. Illarionov, F. Ducry, C. Schleich, S. Wachter, K. Watanabe, T. Taniguchi, T. Mueller, M. Walt, M. Lanza, M. I. Vexler, M. Luisier and T. Grasser, The performance limits of hexagonal boron nitride as an insulator for scaled CMOS devices based on two-dimensional materials. *Nat. Electron.* 4, 98–108 (2021)
[33] M. A. Noras and W. A. Maryniak, Monitoring of electric potential of semiconductor wafer, *Phys. Stat. Sol. (c)* 5, No. 4, 935–938 (2008)
[34] H. Amjadi, The mechanism of voltage decay in corona-charged layers of silicon dioxide during UV irradiation, *IEEE Transactions on Dielectrics and Electrical Insulation*, **7**(2) 222 – 228 (2000)
[35] R. Wild, J. Benduhn and L. Stollenwerk, Surface charge transport and decay in dielectric barrier discharges, *J. Phys. D: Appl. Phys.* 47 435204 (2014)
[36] J. Kindersberger, C. Lederle, Surface charge decay on insulators in air and sulfurhexafluorid - part I: simulation, *IEEE Transactions on Dielectrics and Electrical Insulation,* **15** (4), 941-948 (2008)
[37] S. Lin, L. Xu, L. Zhu, X. Chen, and Z. L. Wang, Electron Transfer in Nanoscale Contact Electrification: Photon Excitation Effect, *Adv. Mater.* **31** 1901418 (2019)
[38] S. Lin, L. Xu, C. Xu, X. Chen, A. C. Wang, B. Zhang, P. Lin, Ya Yang, H. Zhao, Z. Lin Wang, Electron Transfer in Nanoscale Contact Electrification: Effect of Temperature in the Metal–Dielectric Case, *Adv. Mater.* **31**, 1808197 (2019)
[39] L. Giordano, P. V. Sushko, G. Pacchioni, and A. L. Shluger, Electron Trapping at Point Defects on Hydroxylated Silica Surfaces, *Phys. Rev. Lett.* **99**, 136801 (2007)
[40] J. A. Sedlacek, E. Kim, S. T. Rittenhouse, P. F. Weck, H. R. Sadeghpour, and J. P. Shaffer, Electric Field Cancellation on Quartz by Rb Adsorbate-Induced Negative Electron Affinity, *Phys. Rev. Lett.* **116**, 133201 (2016)
[41] F. Buonocore, A. Capasso, M. Celino, N. Lisi, and O. Pulci, Tuning the Electronic Properties of Graphane via Hydroxylation: An Ab Initio Study, *J. Phys.Chem.C* ,**125**,16316−16323 (2021)
[42] Jack Strand, M. Kaviani, D. Gao, A. El-Sayed, V. V. Afanas'ev and A. L. Shluger, Intrinsic charge trapping in amorphous oxide films: status and challenges, *J. Phys.: Condens. Matter* **30** 233001 (2018)

[43] K. P. Loh, I. Sakaguchi, M. N. Gamo, S. Tagawa, T. Sugino, T. Ando; Surface conditioning of chemical vapor deposited hexagonal boron nitride film for negative electron affinity. *Appl. Phys. Lett.* **74** (1): 28–30 (1999)

[44] A. Kimmel, P. Sushko, A. Shluger and G. Bersuker, Positive and Negative Oxygen Vacancies in Amorphous Silica, *ECS Trans.* **19** 3 (2009)